Results for the C5G7 Benchmark Problem Using a Subelement Option of the Variational Nodal Method

M. A. Smith*, N. Tsoulfanidis
University of Missouri, Rolla
Department of Nuclear Engineering
Rolla, Missouri 65409

E. E. Lewis
Northwestern University
Department of Mechanical Engineering
Evanston, Illinois 60208

G. Palmiotti & T. A. Taiwo
Argonne National Laboratory
9700 South Cass Avenue
Argonne, Illinois 60439

ABSTRACT

Recently, an OECD benchmark problem was proposed to test the abilities of modern reactor physics codes to perform three-dimensional transport calculations without spatial homogenization of the fuel-coolant interfaces. To solve this benchmark problem we used the Argonne National Laboratory nodal transport code, VARIANT. VARIANT solves the even-parity transport equation on a nodal grid coupled with odd-parity Lagrange multipliers at the node interfaces. Each spatial node thus constitutes a primal hybrid finite element, with separate spatial approximations within the node and along the interface. The angular variables in the transport equation are treated with an expansion in either spherical harmonics or simplified spherical harmonics.

To treat the spatial heterogeneities defined in the benchmark problem, we replaced the basis set of spatial polynomial trial functions used previously in VARIANT with a finite element spatial approximation. This approach subdivides the spatial node into finite elements with continuous, piecewise linear or quadratic trial functions; we refer to them as subelements. By allowing step changes in cross sections at the subelement interfaces, the spatial heterogeneities within the node can be treated explicitly. Using this new form of the VARIANT code we solved the two-dimensional and three-dimensional problems specified by the OECD benchmark and compared the results to reference multigroup Monte Carlo solutions.

---

* Now At Argonne National Laboratory

1. INTRODUCTION

Present day nodal methods have been used extensively to perform whole-core reactor physics calculations.[1-3] Whether they be nodal diffusion or nodal transport methods, almost all of the nodal methods utilize homogenized cross sections for fuel assembly-size nodes. With constantly improving computer technology, the use of nodal transport approximations for whole-core geometries is becoming more widely feasible and desirable. The largest remaining uncertainties in such calculations most frequently revolve around the use of the homogenized cross sections and the subsequent dehomogenization procedures needed to reconstruct fuel pin powers. To eliminate the need for homogenized nodes, we introduce a subelement formulation of the variational nodal method embodied in the Argonne National Laboratory code VARIANT.[4,5] In VARIANT, the multigroup even-parity transport equation is solved for two- and three-dimensional Cartesian and hexagonal node geometries where the nodes are coupled together using odd-parity spherical harmonic (P_N) or simplified spherical harmonic (SP_N) Lagrange multipliers.

The generalized method we present here retains the response matrix formalism in VARIANT, but replaces the spatial polynomial trial functions within the node with a finite element approximation. The finite element approximation allows the cross sections to be discontinuous at the finite element interfaces, thus the requirement that the nodes be homogeneous is eliminated. To avoid confusion, we have chosen to designate the finite elements as subelements, since the variational nodal method itself may be viewed as a hybrid finite element formulation.[6] To demonstrate the capabilities of the method we present results for a recent OECD benchmark problem[7] in which we implement the subelement approximation for a heterogeneous pin-cell lattice. In Sec. II, the subelement theory is discussed and in Sec. III the results of the two-dimensional benchmark calculations are presented.

2. THEORY

The variational nodal method is a standard multigroup formulation starting with the within-group transport equation

$$\hat{\Omega}\cdot\vec{\nabla}\psi(\vec{r},\hat{\Omega})+\Sigma_t(\vec{r})\psi(\vec{r},\hat{\Omega})=\Sigma_s(\vec{r})\phi(\vec{r})+S(\vec{r}), \tag{1}$$

where we have assumed isotropic scattering and sources. In Eq. (1), $\psi(\vec{r},\hat{\Omega})$ and $\phi(\vec{r})$ represent the group angular and scalar flux, $S(\vec{r})$ is the group source, and $\Sigma_t(\vec{r})$ and $\Sigma_s(\vec{r})$ are the total and within-group scattering cross sections. Equation (1) can be transformed into the second-order even-parity form

$$\hat{\Omega}\cdot\nabla\Sigma_t^{-1}\,\hat{\Omega}\cdot\vec{\nabla}\psi^{+}(\vec{r},\hat{\Omega})+\Sigma_t\,\psi^{+}(\vec{r},\hat{\Omega})=\Sigma_s\,\phi(\vec{r})+S(\vec{r}), \tag{2}$$

where the even- and odd-parity flux components are defined by

$$\psi^{\pm}(\vec{r},\hat{\Omega})=\frac{1}{2}\Big[\psi(\vec{r},\hat{\Omega})\pm\psi(\vec{r},-\hat{\Omega})\Big]. \tag{3}$$

To obtain a nodal form we first write Eq. (2) in a functional form with odd-parity boundary conditions given by

$$F\left[\psi^{+}\right]=\int dV\int d\Omega\left[\Sigma_{t}^{-1}\left(\hat{\Omega}\cdot\vec{\nabla}\psi^{+}\right)^{2}+\psi^{+}\Sigma_{t}\psi^{+}\right]-\int dV\left(\phi\,\Sigma_{s}\phi+2\phi S\right)$$
$$+2\int d\Gamma\int d\Omega\hat{\Omega}\cdot\hat{n}\,\psi^{+}\psi^{-} \tag{4}$$

In Eq. (4), V is the problem domain bounded by the surface Γ with outward normal $\hat{n}$. Upon decomposition of the problem domain V into subdomains V_{ν} (called nodes) we obtain the nodal functional

$$F_{\nu}\left[\psi^{+},\psi^{-}\right]=\int_{\nu}dV\int d\Omega\left[\Sigma_{t}^{-1}\left(\hat{\Omega}\cdot\vec{\nabla}\psi^{+}\right)^{2}+\psi^{+}\Sigma_{t}\psi^{+}\right]-\int_{\nu}dV\left[\phi\,\Sigma_{s}\phi+2\phi S\right]$$
$$+2\int_{\nu}d\Gamma\int d\Omega\left[\hat{\Omega}\cdot\hat{n}\,\psi^{+}\psi^{-}\right] \tag{5}$$

with the odd parity flux continuity equation

$$F\left[\psi^{+},\psi^{-}\right]=\sum_{\nu}F_{\nu}\left[\psi^{+},\psi^{-}\right], \tag{6}$$

Note that at each node interface the even-parity flux $\psi^{+}(\vec{r},\hat{\Omega})$ is allowed to be discontinuous while the odd-parity flux $\psi^{-}(\vec{r},\hat{\Omega})$ is not.

To implement the subelement treatment, we subdivide the nodal volume into finite elements with volume V_{e}. Figure 1 shows an example of a subdivision of a two-dimensional Cartesian node into triangular finite elements.

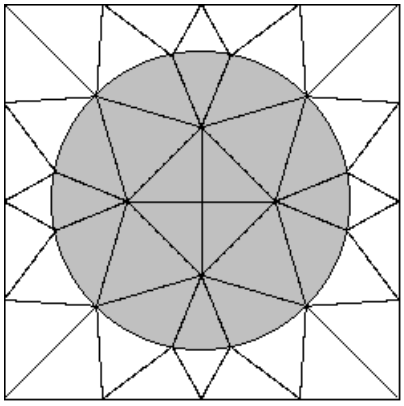

Figure 1. Finite Element Mesh Approximation

The nodal functional in Eq. (6) can be written as a superposition of subelement functionals

$$F_{\nu}\left[\psi^{+},\psi^{-}\right]=\sum_{e}F_{(e)}\left[\psi_{e}^{+},\psi^{-}\right], \tag{7}$$

where the functional for each subelement is given as

$$F_{(e)}\left[\psi_e^+,\psi^-\right]=\int_{(e)}dV\int d\Omega\left[\Sigma_{t,e}{}^{-1}\left(\hat{\Omega}\cdot\vec{\nabla}\psi_e^+\right)^2+\psi_e^+\Sigma_{t,e}\,\psi_e^+\right]$$
$$-\int_{(e)}dV\left[\phi_e\,\Sigma_{s,e}\phi_e+2\phi_e S_e\right]+2\int_{(e)}d\Gamma\int d\Omega\hat{\Omega}\cdot\hat{n}\,\psi_e^+\psi^- \qquad (8)$$

In this work we only consider finite element basis functions that are continuous across subelement interfaces, thus the surface term in Eq. (8) only appears along the nodal interfaces and, consequently, only for those subelements adjacent to nodal interfaces. The spatial and angular approximation of the flux within each subelement is

$$\psi_e^+\left(\vec{r},\hat{\Omega}\right)=\mathbf{g}^T(\hat{\Omega})\otimes\mathbf{f}^T(\vec{r})\,\xi_e,\qquad \vec{r}\in V_e \qquad (9)$$

while the source is

$$S_e\left(\vec{r}\right)=\mathbf{f}^T(\vec{r})\,\mathbf{s}_e, \qquad (10)$$

and the odd-parity flux along each nodal interface γ is

$$\psi^-\left(\vec{r},\hat{\Omega}\right)=\mathbf{k}_\gamma^T(\hat{\Omega})\otimes\mathbf{h}_\gamma^T(\vec{r})\,\chi_\gamma.\qquad \vec{r}\in\Gamma_\nu \qquad (11)$$

Here the symbol $\otimes$ indicates Kronecker tensor multiplication of the angular and spatial trial functions, and ξ_e and χ_γ are the unknown coefficients. The even- and odd-parity angular functions $\mathbf{g}(\hat{\Omega})$ and $\mathbf{k}_\gamma(\hat{\Omega})$ are vectors of spherical harmonics defined such that Rumyantsev boundary conditions[8] are satisfied across the nodal interfaces. The spatial dependence, $\mathbf{h}_\gamma(\vec{r})$, of the odd-parity Lagrange multiplier is approximated with a set of orthogonal polynomials detailed in earlier work.[4] The spatial distribution of the even-parity flux, $\mathbf{f}(\vec{r})$, is given by the finite element trial functions where the cross sections are assumed to be unique constants within each finite element.

After Insertion of Eqs. (9), (10) and (11) into Eq. (8), we arrive at the algebraic functional for each subelement

$$F_e\left[\xi_e,\chi_\gamma\right]=\xi_e^T\left(\sum_{K,L}\mathbf{H}^{K,L}\otimes\Sigma_{t,e}^{-1}\mathbf{P}^{K,L,e}+\mathbf{I}\otimes\Sigma_{t,e}\mathbf{F}^e-\mathbf{K}\otimes\Sigma_{s,e}\mathbf{F}^e\right)\xi_e$$
$$-2\xi_e^T\left(\mathbf{K}\otimes\mathbf{F}^e\mathbf{s}_e\right)+2\sum_{\gamma'}\xi_e^T\left(\mathbf{E}_{\gamma'}\otimes\mathbf{D}_{\gamma'}^e\right)\chi_{\gamma'} \qquad (12)$$

where the matrices resulting from the spatial and angular integrations are described elsewhere.[4] To assemble the nodal functional and impose continuity across each finite element interface, we map the local finite element trial function coefficients, ξ_e, into a nodal vector of coefficients ζ. This Boolean transformation relation is expressed as

$$\xi_e=\Xi_e\zeta, \qquad (13)$$

where Ξ_e is a Boolean matrix, a description for which can be found in standard finite element literature.

The introduction of Eq. (13) into Eq. (12) and subsequent substitution into Eq. (7) yields

$$F_v\left[\zeta,\chi\right]=\zeta^T\mathbf{A}\zeta-2\zeta^T\mathbf{s}+2\sum_{\gamma'}\zeta^T\mathbf{M}_{\gamma'}\chi_{\gamma'}\,, \tag{14}$$

where

$$\mathbf{A}=\sum_{K,L}\mathbf{H}^{K,L}\otimes\sum_e\Xi_e^T\Sigma_{t,e}^{-1}\mathbf{P}^{K,L,e}\Xi_e+\mathbf{I}\otimes\sum_e\Xi_e^T\Sigma_{t,e}\mathbf{F}^e\Xi_e-\mathbf{K}\otimes\sum_e\Xi_e^T\Sigma_{s,e}\mathbf{F}^e\Xi_e\,, \tag{15}$$

$$\mathbf{s}=\mathbf{K}\otimes\sum_e\Xi_e^T\mathbf{F}^e\mathbf{s}_e\Xi_e\,, \tag{16}$$

$$\mathbf{M}_\gamma=\mathbf{E}_\gamma\otimes\sum_e\Xi_e^T\mathbf{D}_\gamma^e\,, \tag{17}$$

and $\mathbf{I}$ Is the identity matrix. With the detail of the subelement spatial approximation completed within each node, we find that the form of Eq. (14) is identical to that of previous work and therefore so are the remaining equations in the response matrix formulation. For brevity we simply state the resulting response matrix equations

$$\mathbf{j}^+=\mathbf{R}\,\mathbf{j}^-+\mathbf{B}\mathbf{s} \tag{18}$$

and

$$\zeta=\mathbf{A}^{-1}\mathbf{s}-\mathbf{A}^{-1}\mathbf{M}\left(\mathbf{j}^+-\mathbf{j}^-\right). \tag{19}$$

An additional approximation implemented in conjunction with the subelement approximation is source lumping. Instead of using a consistent source, as that defined by Eq. (10), we lump or average the source over several contiguous elements with identical cross sections.[9] This technique has two major benefits: (a) the number of source components is reduced, thus reducing the computational burden of the fission source iterations, and (b) the lumped source components are found to converge faster than the components of the consistent source during the fission source iterations.

3. RESULTS

We have modified the VARIANT code to accommodate the subelement formulation and employed it to solve the two-dimensional benchmark problem specified by OECD.[7] This benchmark problem was formulated to test the accuracy of the space-angle approximations implemented in deterministic transport codes. The configuration of the benchmark problem is detailed elsewhere along with our studies on convergence of the various angular and spatial approximations.[9] In this work we display a subset of the results we have obtained using a 48 subelement approximation of the pin-cell geometry shown in Fig. 1, which we have found to be a sufficiently converged spatial approximation of the pin-cell geometry. Each subelement in Fig. 1 has quadratic basis functions yielding a total of 113 spatial degrees of freedom per node. We have devised three lumped source approximations: 2, 5, and 8, as indicated in Fig. 2.

We first investigate the convergence behavior of the benchmark eigenvalue with respect to the spherical harmonic angular approximation using Figures 3 and 4.

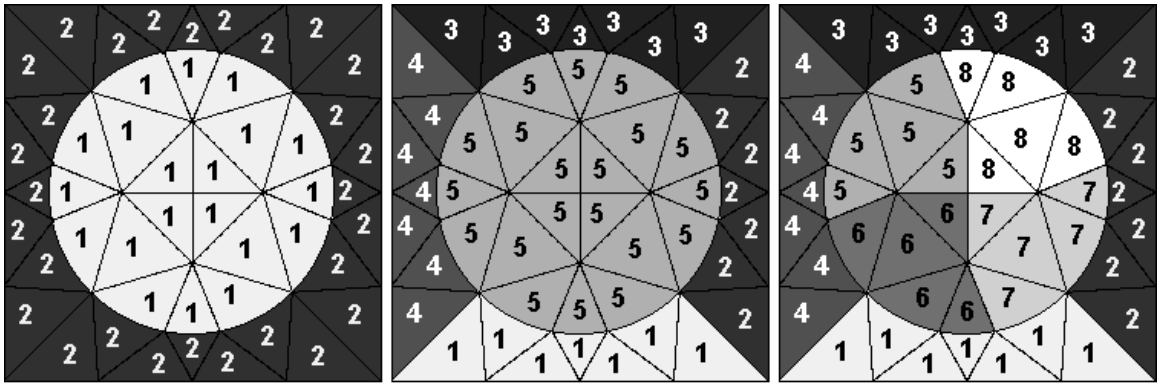

Figure 2. Two, Five, and Eight Lumped Source Representations of the Pin-cell Geometry

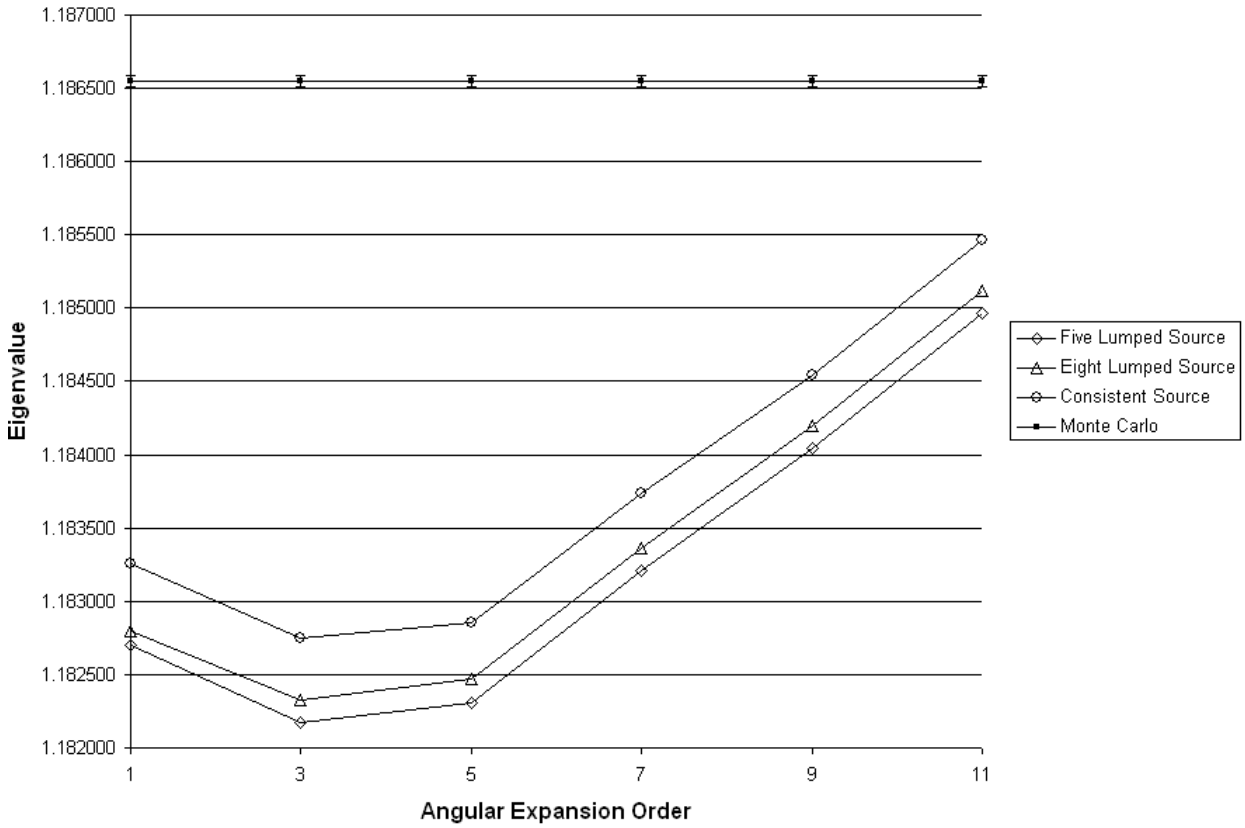

Figure 3. Eigenvalue Behavior of Different Source Approximations.

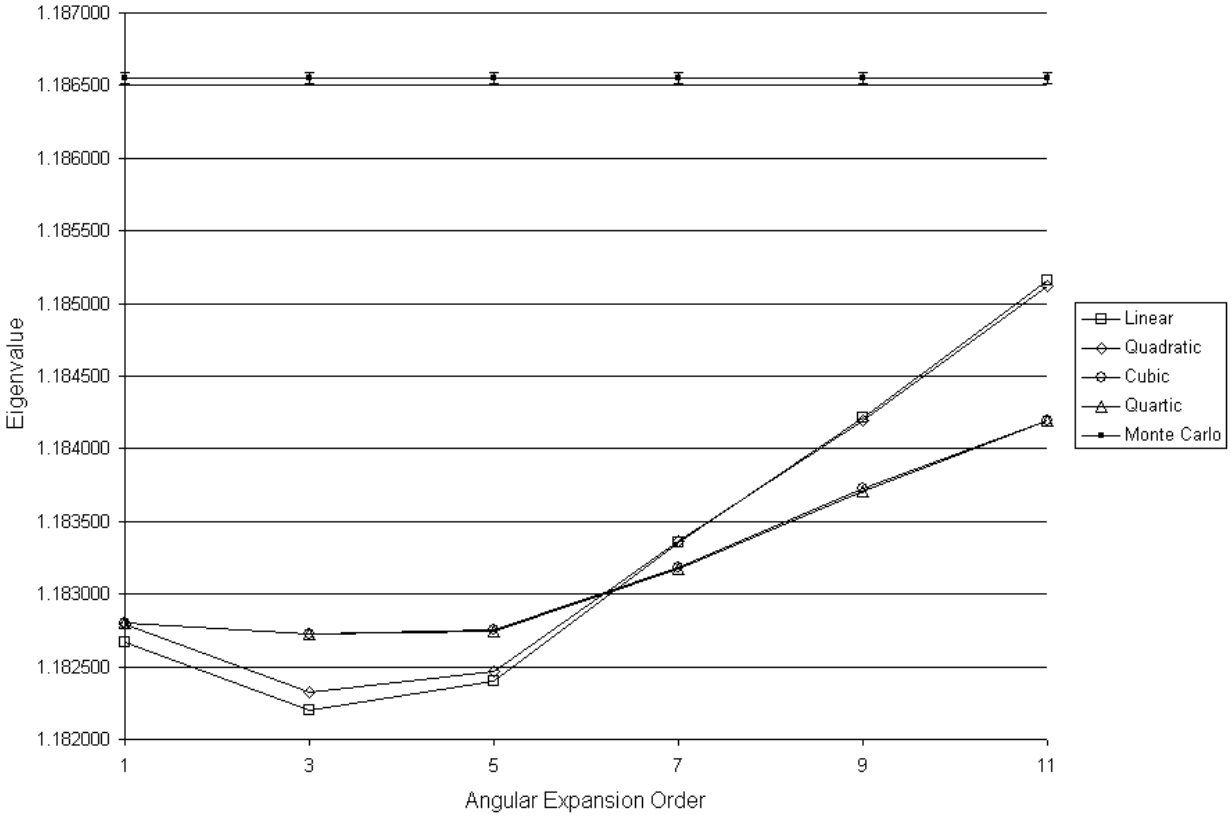

Figure 4. Eigenvalue Behavior of Different Lagrange Multiplier Approximations.

Figures 3 and 4 show that all of the VARIANT solutions converge towards the reference MCNP[10] solution as the order of the angular approximation is refined. Convergence with respect to the angular approximation, however, is quite slow, and even the P_{11} results indicate that substantially more refinement is necessary to come within the error bars of the Monte Carlo solution. In other work[9] we have estimated that an angular approximation on the order of P_{25} may be necessary to obtain Monte Carlo level of accuracy, while at present our computational capabilities will allow no higher than P_{15} solutions to be undertaken.

The lumped source approximation poses an additional level of approximation implemented in our present method. To examine the resulting loss in accuracy, we have obtained benchmark solutions using a 5-lumped, an 8-lumped, and a consistent source approximation. The results plotted in Fig. 3 indicate the degree of accuracy lost in the eigenvalue solution. The error is roughly independent of the angular approximation and is relatively minor compared to that accrued through the use of an inadequate angular approximation. The major advantage of the lumped source approximation is the CPU time reduction; the 8-lumped source approximation is 50 times faster than the consistent source. Therefore, provided the losses in accuracy for the eigenvalue and fission source distribution are acceptable, the lumped source approximation is very beneficial. Further refinement of the lumped source approximation to values between 8 and

48 regions has been found to provide only marginal improvements in accuracy over the 8-lumped source approximation while adding considerably to the computational burden.

The results in Fig. 4 show the sensitivity of the eigenvalue to refinements in the Lagrange multiplier approximation. Linear through quadric approximations are included; the flat approximation results are, in general, too poor to warrant consideration. In earlier work[9] the effect of using a consistent finite element approximation was investigated and it was found that virtually no improvement was gained for Lagrange multiplier approximations greater than cubic. Figure 4, however, indicates that the eigenvalue has not converged with respect to Lagrange multiplier order, especially for high order angular approximations. We have found that the gains from using higher-order Lagrange multiplier expansions are not as significant as the effect of improving the angular approximation.

The accuracy of the VARIANT pin power results can be summarized by tabulating the following three quantities: the percent error of the pin with the maximum power, the maximum pin power percent error, and the root mean square (RMS) error of the pin power distribution. These results, along with the eigenvalue errors, are presented in Tables I and II.

Table I. Percent Errors for the P_N Angular, 8-lumped Source, Quadratic Lagrange Multiplier Approximation

Angular Order	Eigenvalue	Maximum Pin Power	Maximum	RMS
P_1	-0.316	0.604	6.437	1.766
P_3	-0.356	0.795	1.918	0.704
P_5	-0.344	0.374	1.214	0.379
P_7	-0.268	-0.021	0.948	0.225
P_9	-0.199	-0.230	0.969	0.272
P_{11}	-0.121	-0.443	1.221	0.389
P_{13}	-0.070	-0.572	1.372	0.472
MCNP Reference	±0.003	±0.070	±0.250	0.145

Table I shows the errors for the 48 subelement mesh using an 8-lumped source and quadratic Lagrange multiplier approximation, while Table II gives the errors for a consistent source approximation and a cubic Lagrange multiplier approximation. In both tables, the MCNP reference values represent the 68% confidence intervals associated with the reference solution power distribution.

Table II. Percent Errors for the P_N Angular, Consistent Source, Cubic Lagrange Multiplier Approximation

Angular Order	Eigenvalue	Maximum Pin Power	Maximum	RMS
P_1	-0.278	0.942	5.911	1.726
P_3	-0.287	1.348	2.259	1.023
P_5	-0.286	0.995	1.797	0.763
P_7	-0.250	0.751	1.532	0.588
P_9	-0.205	0.583	1.345	0.470
P_{11}	-0.166	0.468	1.214	0.393
P_{13}	-0.135	0.394	1.124	0.344
MCNP Reference	±0.003	±0.070	±0.250	0.145

Asymptotic convergence of the pin power solutions appears to be present in Table II, but not Table I. The lack of asymptotic convergence can be traced to error cancellation between the Lagrange multiplier and lumped source approximations in some of the lower-order spherical harmonic approximations. This is most clearly seen in Table I by the sign change in the third column (the percent error for the pin with the maximum power) between the P_5 and P_7 angular approximations. The other two pin power percent error measures are also found to reach a minimum between P_5 and P_7. Since error cancellation cannot be relied upon to obtain accurate solutions, we employ more refined source and interface approximations as seen in Table II. The results in Table II are the most accurate that we have obtained to date with this method. Computational costs would escalate dramatically were the remaining inaccuracies in eigenvalue and power distribution to be resolved by further refining the angular and Lagrange multiplier approximations.

CONCLUSIONS

The above results demonstrate that the subelement treatment implemented in the variational nodal framework is a viable method for solving two-dimensional core problems without spatial homogenization. For the chosen benchmark problem, the method's primary limitation is the computational expense incurred in using very high order spherical harmonics approximations required to gain agreement with the reference Monte Carlo solutions. At present, however, the computational algorithms of the subelement feature of the VARIANT code have not been optimized nor have acceleration methods been considered. Nevertheless, even the most accurate VARIANT solution still required less than 1/3 of the CPU time as that of the reference MCNP solution. The subelement formulation has been generalized to three dimensions, and work is progressing on generating solutions for the three-dimensional OECD benchmark problem. Such problems, in which spatial homogenization has been removed at the pin-cell level, present particularly severe challenges to present-day transport computational methods. For other classes of problems the subelement formulation contained herein may provide an attractive approach for treating heterogeneous nodes in multidimensional transport problems.

ACKNOWLEDGEMENTS

This work is based, in part, on a dissertation submitted by the first author in partial fulfillment of the PhD requirements at the University of Missouri-Rolla. It was supported by the U.S. Department of Energy under Contract number W-31-109-ENG-38 and by the U.S. Department of Energy Contract number DE-FG07-98ID13632.

REFERENCES

1. M. R. Wagner and K. Koebke, "Progress in Nodal Reactor Analysis," *Proc. Topl. Mtg. Advances in Reactor Computations,* Salt Lake City, Utah, March 28-31, 1983, Vol. II, p. 941, American Nuclear Society (1983).

2. D. Lawrence, "Progress in Nodal Methods for the Solution of the Neutron Diffusion and Transport Equations," *Prog. Nucl. Energy*, **17**, 271 (1986).

3. A. Badruzzaman, "Nodal Methods in Transport Theory," *Adv. Nuclear Science and Technology,* Vol. 21, J. Lewins and M. Becker, editors, Plenum Press, New York (1990).

4. G. Palmiotti, E. E. Lewis, C. B. Carrico, "VARIANT: VARIational Anisotropic Nodal Transport for Multidimensional Cartesian and Hexagonal Geometry Calculation," *Argonne National Laboratory* ANL-95/40, 1995.

5. C. B. Carrico, E.E. Lewis and G. Palmiotti, "Three Dimensional Variational Nodal Transport Methods for Cartesian, Triangular and Hexagonal Criticality Calculations," *Nucl. Sci. Eng.* **111**, 168 (1992).

6. E. E. Lewis, G. Palmiotti, and T. Taiwo, "Space-Angle Approximations in the Variational Nodal Method," *Proc. Int. Conf. Mathematics and Computations, Reactor Analysis and Environmental Analysis in Nuclear Applications*, Vol. 1, **827**. September 27-30, Madrid, Spain (1999).

7. E. E. Lewis, G. Palmiotti, T. A. Taiwo, M. A. Smith, & N. Tsoulfanidis, "Benchmark Specification for Deterministic 2-D/3-D MOX Fuel Assembly Transport Calculations without Spatial Homogenization (C5G7 MOX)," *NEA/NSC/DOC(2001)4*, March 28, 2001.

8. G. Ya. Rumyantsev, "Boundary Conditions in the Spherical Harmonic Method," *J. Nucl. Energy*, **16**, 111 (1962).

9. M. A. Smith, "Implementation of the Finite Element Approximation in a Nodal Three-Dimensional Transport Program to allow for Explicit Node Geometries," PhD dissertation, University of Missouri-Rolla (2001).

10. Judith F. Briesmeister and XTM. "MCNP^{TM}-A General Monte Carlo N-Particle Transport Code." *LOS ALAMOS National Laboratory LA-12625-M*, March 1997.